2 June 2000

ELSEVIER

Chemical Physics Letters 322 (2000) 579–586

CHEMICAL PHYSICS LETTERS

www.elsevier.nl/locate/cplett

Exact computation of the triply periodic Schwarz *P* minimal surface

Paul J.F. Gandy, Jacek Klinowski *

Department of Chemistry, University of Cambridge, Lensfield Road, Cambridge CB2 1EW, UK

Received 23 March 2000; in final form 10 April 2000

Abstract

Parametrization of the Schwarz *P* triply periodic minimal surface, found in many physical, chemical and biological systems, has allowed us to calculate its coordinates analytically, and to describe its properties, such as the surface-to-volume ratio. Real structures may now be quantitatively compared with the precise coordinates and quantified in terms of the surface parameters.

1. Introduction

A minimal surface is a surface for which the mean curvature $H=(k_1+k_2)/2$ is zero at every point, where k_1 and k_2 are the principal curvatures [1]. A triply periodic minimal surface (TPMS) is a minimal surface which is periodic in three independent directions. TPMS are omnipresent in the natural and man-made worlds and provide a concise description of many seemingly unrelated structures [2]. They have become of interest not only to the structural chemist, but also the biologist [3], structural engineer and the materials scientist [4], and are echoed in art and architecture [5]. The Schwarz *P* surface (colloquially known as 'the plumber's nightmare') is found in the ternary mixtures of oil, water and surfactant. These self-assembled structures are templates in the inorganic and organic polymerisation reactions which lead to mesoporous molecular sieves [6,7] and contact lens materials [8], respectively. Other cubic phases are found in ternary mixtures of surfactants with oil and water [9]. In the system of didodecyldimethylammonium bromide–water–styrene, periodic surfaces exist over a wide range of water fractions. The *P* surface is also found in the zeolite sodalite, $Na_4Al_3Si_{12}O_{26}Cl$, and the perovskite-type structure of $CaTiO_3$ [10]. The periodic zero equipotential surface [11] called P^* in compounds with the caesium chloride structure is the topological analogue of the *P* surface.

Following the discovery of new carbon architectures (fullerenes, tubes and spirals), it has been shown that TPMS can be 'decorated' with carbon atoms [12]. Hypothetical ordered graphite foams with topologies similar to periodic minimal surfaces have

* Corresponding author. Fax: +44-1223-336362; e-mail: jk18@cam.ac.uk

0009-2614/00/$ - see front matter
PII: S0009-2614(00)00453-X

been constructed by introducing 7- or 8-membered rings of carbon atoms into sheets of 6-membered rings so as to give rise to saddle-shape surfaces [13]. These structures should be more stable than fullerenes mainly because the 120° bond angles in graphite are almost preserved. The energies of the *P*, *D*, *G* and *I-WP* surfaces decorated with carbon were found to be lower than that of the C_{60} molecule.

The presence of periodic surfaces in plant etioplasts and in the course of crystallisation of membrane proteins [14] indicates their morphogenetic function. When a plant is grown in the absence of light, the lamellar structure of chloroplasts (organella involved in photosynthesis) transforms into the periodic surface of the same topology and symmetry as the *P* surface, although not minimal [15]. Cell membranes in living organisms, such as the endoplasmic reticulum and the cellular organella, have complex three-dimensional morphologies, which correspond to those of the *P*, *G* and *D* surfaces [16]. The skeletal elements of sea stars, sea urchins and sea-cucumbers are the monocrystals of a magnesium-rich calcite, each crystal being delimited by a surface with the same topology as the *P* surface rather than a planar surface [3]. The periodic structures formed by lipids, surfactants and soaps in water solutions have been known since 1967 [17].

In all real structures, minimal surfaces have been identified by visual inspection – in a way which is anecdotal rather than quantitative. In order to be able to compare real structures (for example, those stored in the Cambridge Crystallographic Database) with TPMS, it is necessary to know the precise coordinates of the latter. With this in mind, we have given analytical expressions for the parameters and the *D* [18] and *G* [19] surfaces using our analytical equations for the *tD* surfaces [20]. The aim of this work is to give such expressions for the *P* surface.

2. Enneper–Weierstrass representation

A minimal surface free of self-intersections is said to be embedded. TPMS are described in terms of the fundamental patch ('Flächenstück'): the smallest portion of the surface from which the entire surface can be constructed. The Enneper–Weierstrass representation [21] gives the coordinates of a minimal surface as

$$x = \mathrm{Re}e^{i\theta}\int_{\omega_o}^{\omega}(1-\tau^2)\,R(\tau)\,\mathrm{d}\tau,$$

$$y = \mathrm{Re}e^{i\theta}\int_{\omega_o}^{\omega}i(1+\tau^2)\,R(\tau)\,\mathrm{d}\tau,$$

$$z = \mathrm{Re}e^{i\theta}\int_{\omega_o}^{\omega}2\tau R(\tau)\,\mathrm{d}\tau, \qquad (1)$$

where $i^2=-1$ and $\tau=\tau_a+i\tau_b$, associating with function $R(\tau)$ (the Weierstrass function) a unique surface $r(\tau_a,\tau_b)$ which is guaranteed to be minimal; θ is the so-called Bonnet angle. The Cartesian coordinates of any point are expressed as the real parts (Re) of contour integrals, evaluated in the complex plane from some fixed point ω_o to a variable point ω. A specific minimal surface can be determined by integrating its Weierstrass function. The integrals (1) can always be evaluated by numerical integration, but so far have been calculated analytically for only a few surfaces [18–20,22–25].

Using the Bonnet transformation, fully described by the Bonnet angle, we can generate from a minimal surface a family of minimal surfaces with the same metric and Gaussian curvatures. By changing θ we obtain associate surfaces; when $\theta=\pi/2$, the associate surface is known as the conjugate surface. With respect to the *D* surface, the Bonnet angles are $\theta=90°$ (for the *P* surface) and $\theta=\mathrm{ArcCot}[K'/K]=38.0147°$, where $K=\mathrm{EllipticK}[1/4]$ and $K'=\mathrm{EllipticK}[3/4]$ (for the *G* surface) [26].

The generating space group of the *P* surface is $Pm\bar{3}m$ (No. 221) and the symmetry of the surface is $\mathrm{Im}\bar{3}m$ (No. 229) which contains 48 equivalent positions. It is thus possible to divide the unit cell into 48 equivalent asymmetric volumes related by the symmetry elements of its space group. The surface embeds an inversion centre together with two-fold lines which interchange the two sides of the surface and also the two labyrinth networks which it partitions. The pair of labyrinths of the *P* surface are 6-connected and are simply related by translation. TPMS such as *P*, *D* and *G* divide space into two equal, but

some (*I-WP*, *O* and *C-TO*) into unequal subvolumes.

Although the properties of the TPMS follow uniquely from the Weierstrass function, $R(\tau)$ [20], the function is known only for several TPMS of simple topology. The Weierstrass function may be constructed if there exists a surface patch from which the whole TPMS can be generated by reflection or rotation of the patch using appropriate symmetry elements [20]. This is the case for the *D*, *G* and *P* surfaces, for which the Weierstrass function is [27]

$$R(\tau) = \frac{1}{\sqrt{\tau^8 + \lambda\tau^4 + 1}} \qquad (2)$$

with $\lambda = -14$.

In general, the Weierstrass function is specified by values of τ which correspond to flat ('umbilical') points on the minimal surface where the Gaussian curvature is zero, in a form $\Pi_i(\tau - \tau_i)^\eta$, where η determines the topology of the surface. The *P* surface has eight flat points through which three-fold inversion axes run. Around a small circle enclosing a flat point a vector normal to the surface rotates with twice the angular velocity in the counter-rotatory direction. The maxima of $|k_1| = |k_2|$ occur at four points around the nape of each neck in the *P* surface. The flat points, defined as points where every cross-section is inflected and the two principal curvatures become degenerate $|k_1| = |k_2| = 0$, occur periodically on the surface and in the unit cell occur at the eight monkey-saddle points.

The fundamental patch of the *P* surface is inscribed in a quadrirectangular tetrahedron, its four vertices having coordinates proportional to the space vectors $(-1,0,0)$, $(1,-2,0)$, $(1,2,0)$ and $(-1,0,2)$

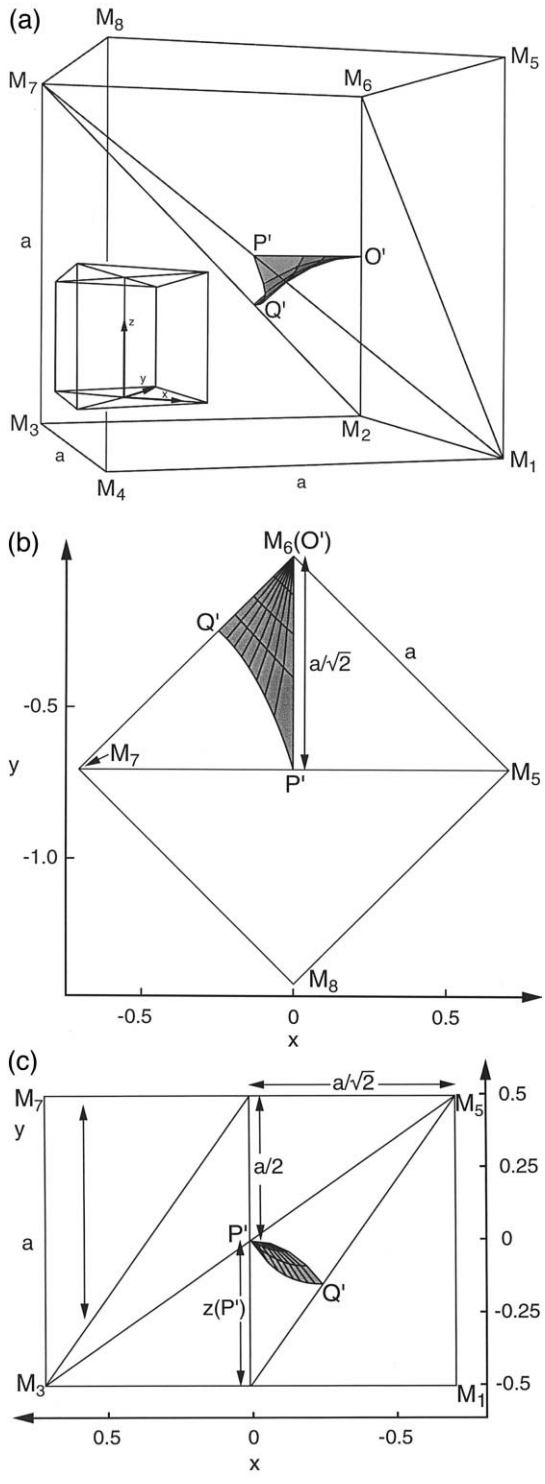

Fig. 1. (a) The fundamental patch of the *P* surface shown within its bounding cell (the cube with edge length *a*). The patch is confined by the tri-rectangular tetrahedron and meets its faces orthogonally. The coordinate system has its origin at point *O′* and its orientation is indicated by the axes shown in the inset diagram. Flat point *O′* divides the cube edge, *a*, in the ratio 1:1. Flat point *P′* divides the body diagonal in the 1:1 ratio. (b) The projection of the patch onto the *xy* plane showing the relationship between the *x* and *y* coordinates of the points *O′*, *P′* and *Q′*. (c) The projection of the patch onto the *zx* plane showing the relationship between the *x* and *z* coordinates of the points *O′*, *P′* and *Q′*.

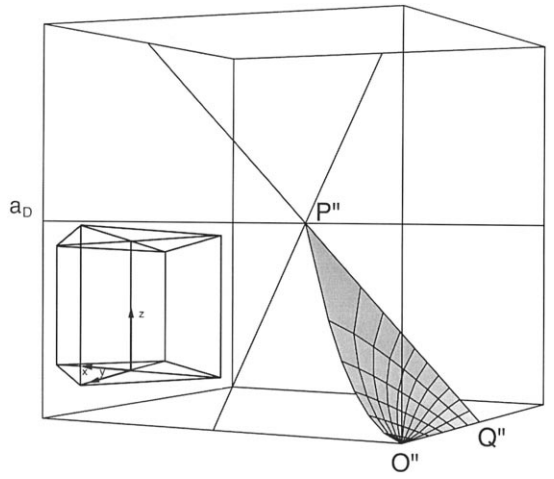

Fig. 2. A patch of the D triply periodic minimal surface (conjugate to P) is bounded by the edges of the quadrirectangular tetrahedron $O''P''Q''R''$. The origin of the coordinate system imposed by the parametrization is at O'' and the orientation of the axes is shown in the inset.

and was so named by Coxeter [28], because its face angles include four right angles (Fig. 1a). This is its kaleidoscopic cell or fundamental region for groups of reflections in R^3, i.e. the convex polyhedron which provides plane boundaries enclosing a finite minimal surface patch which can be replicated by reflection to yield an infinite TPMS without self-intersections. Six of these pieces combine to form a larger surface piece in the hierarchy of assembly, contained within a cube of side a (Fig. 4a), which we will refer to as the bounding cell of the P patch. The boundary of the patch of the P surface is defined by one straight line (Fig. 2) which is an embedded 2-fold axis, and two mirror plane curves. The converse is true for its adjoint twin, the D surface. Apart from the CLP surface and its homeomorphic adjoint, which are identical other than having different tetragonal proportions, the P, D and G surfaces are the only other examples of intersection-free associate TPMS. The effect of the Bonnet transformation is to transform the lattice of catenoidal channels into helicoidal strips, through a screw operation on the whole surface. The P surface contains plane 'holes' which are almost circular in cross-section. Schwarz showed that these have radius variations of only about 0.4% [29]. The four-fold screw isometries collapse to a screw of zero pitch, but finite 'hole' diameter, for P, and reach a limit of finite pitch, but zero 'hole' diameter, for D. The images of these hole curves in P are straight lines in D. The transformation of the quasi-circular holes in P into straight line holes in D, via the intermediate quasi-helical holes of the type which appear in G, is illustrated by the example of the line segment which is shown extending from left to right along the central axis of the fundamental region of D. This line segment corresponds to a single pitch of the general quasi-helical hole curve. The diameter of such a quasi-helix is defined as the diameter of the closely similar circular helix which passes through the vertices of the regular map {6,4|4}.

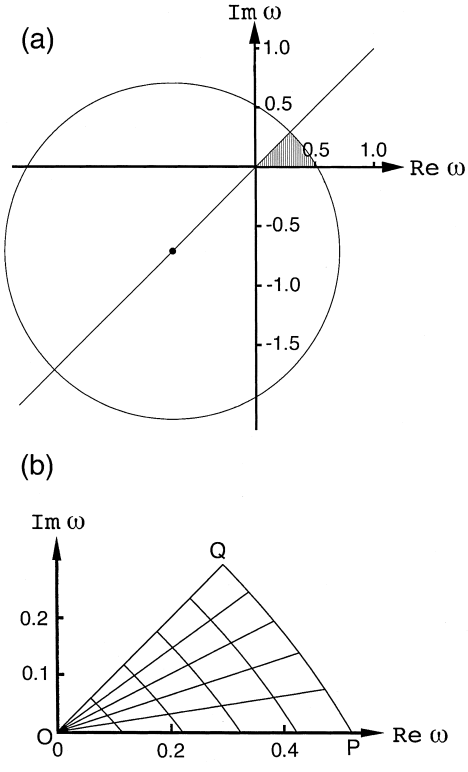

Fig. 3. (a) Integration domain of the P patch (shaded). (b) The mesh used for computing the P surface. The complex-plane coordinates of points O, P and Q are $O(0,0)$, $P((\sqrt{3}-1)/\sqrt{2},0)$ and $Q((\sqrt{2}-1)/2,((\sqrt{2}-1)/2)$. The circular arc which bounds the domain is that of the circle of radius $\sqrt{2}$ centered at $(-\sqrt{2}/2,-\sqrt{2}/2)$. Its centre is marked with a point.

Thus, the quasi-helix may be described as the circum-helix of the regular helical polygon, having a four-fold screw isometry which is a hole of the regular map {6,4|4} in the regular warped polyhedron which is homeomorphic to *G*. The primitive cell of the *P* surface has the same symmetry as the cubic cell and contains 12 *P*-saddles. The integration domain is indicated by the shaded region in Fig. 3.

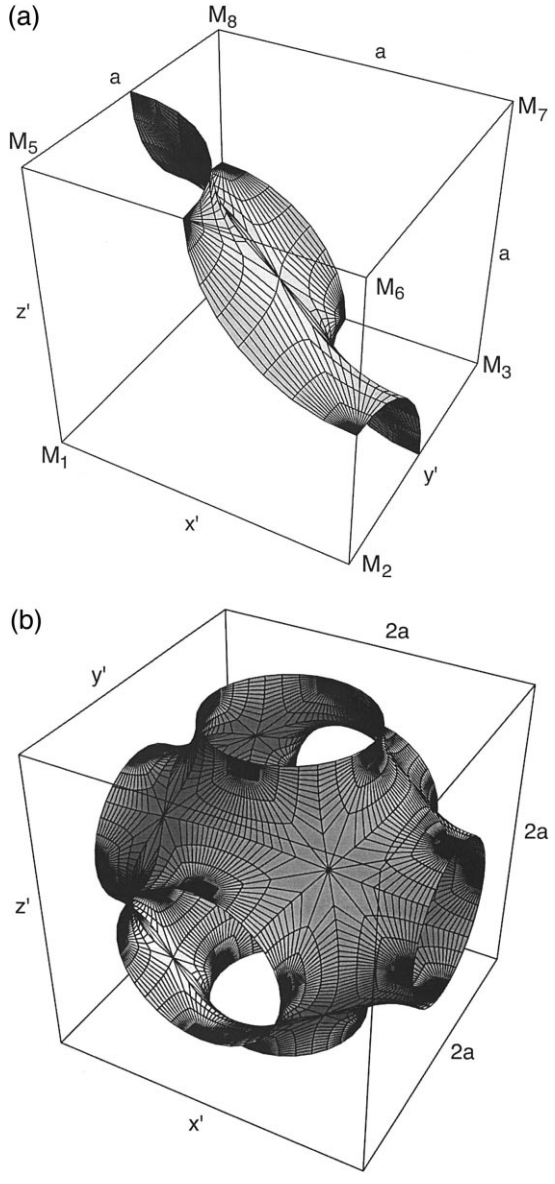

Fig. 4. The transformed coordinate system used in this figure is explained in the text. (a) A piece of the *P* surface composed of six fundamental patches is inscribed in the bounding cell. Six edges of the cube are divided in the 1:1 ratio. (b) The unit cell of the *P* surface made by combining eight pieces shown in (a). The exact surface area of this piece is $12a^2K/K'$. The origin of the coordinate system is at the centre of the cube, and the orientation of the axes is as shown.

Table 1
Cartesian coordinates x', y' and z' of the six fundamental patches which make up the bounding cell of the *P* surface. The coordinates x, y and z are given by Eqs. (5) and (7). To compute the coordinates in the new frame, $\xi = 1/\sqrt{2}$ and $\eta = a/2$

Patch	x'	y'	z'
P_1	$-\zeta x-\zeta y$	$z+\eta$	$-\zeta x+\zeta y+2\eta$
P_2	$-\zeta x-\zeta y$	$-\zeta x+\zeta y+2\eta$	$z+\eta$
P_3	$z+\eta$	$-\zeta x-\zeta y$	$-\zeta x+\zeta y+2\eta$
P_4	$-\zeta x+\zeta y+2\eta$	$z+\eta$	$-\zeta x-\zeta y$
P_5	$-\zeta x+\zeta y+2\eta$	$-\zeta x-\zeta y$	$z+\eta$
P_6	$z+\eta$	$-\zeta x+\zeta y+2\eta$	$-\zeta x-\zeta y$

3. Parametrization of the P surface

Integrals obtained by substituting (2) into (1) and putting $\theta = \pi/2$ and $\omega_o = 0$ can be expressed in terms of the incomplete elliptic integrals of the first kind, $F(\varphi,k^2)$ [30–32]. The modulus k is real and lies in the interval [0,1]. The amplitude φ is complex.

The Cartesian coordinates of any point on the *P* patch are

$$(x,y,z) = \left[\mathrm{Re}(x^*), \mathrm{Re}(y^*), \mathrm{Re}(z^*)\right], \qquad (3a)$$

where

$$x^*(\omega) = I_0 - I_2,$$
$$y^*(\omega) = i(I_0 + I_2),$$
$$z^*(\omega) = 2I_1, \qquad (3b)$$

and the I_p are the integrals

$$I_p(\omega) = I_p(0) + \kappa\int_0^{\omega} \frac{\tau^p \, d\tau}{\sqrt{\tau^8 - 14\tau^4 + 1}}$$

with $p = 0,1$ and 2. (3c)

The variable limit ω is any complex point either inside or on the boundary of the domain shown in Fig. 3. With the double substitution $\tau = t^{1/2}$ and

$s = t + 1/t$, the integrals (3c) are reduced to elliptic integrals [20]. These are expressed in terms of the Legendre–Jacobi integrals to give the surface coordinates as

$$x = -\kappa\,\mathrm{Im}\left\{\frac{1}{2\sqrt{2}}\,\mathrm{EllipticF}\times\left[\mathrm{ArcSin}\left(\frac{2\sqrt{2}\,\omega}{\sqrt{\omega^4+4\omega^2+1}}\right),\frac{1}{4}\right]\right\}, \tag{4a}$$

$$y = \kappa\,\mathrm{Re}\left\{\frac{1}{2\sqrt{2}}\,\mathrm{EllipticF}\times\left[\mathrm{ArcSin}\left(\frac{-2\sqrt{2}\,\omega}{\sqrt{\omega^4+4\omega^2+1}}\right),\frac{3}{4}\right]\right\}, \tag{4b}$$

$$z = -\kappa\,\mathrm{Im}\left\{\frac{1}{4}\,\mathrm{EllipticF}\times\left[\mathrm{ArcSin}\left(\frac{4\omega^2}{\omega^4+1}\right),97-56\sqrt{3}\right]\right\}. \tag{4c}$$

The point $\omega = (\sqrt{3}-1)/\sqrt{2}$ (point Q in Fig. 2b) is a singular point of the Weierstrass function (2). However, in view of (3) the values of $x(Q)$, $y(Q)$ and $z(Q)$ exist and are finite. The point $\omega = 0$ is mapped into (0,0,0). The coordinate frame is therefore defined jointly by the Weierstrass function (2) and the parametrization (see Fig. 1a).

A simple closed-form analytical expression for κ may be derived. The complex-plane coordinate of the point Q is $((\sqrt{3}-1)/\sqrt{2},0)$. Note that when $\omega = (\sqrt{3}-1)/\sqrt{2}$, $\omega^2 = 2-\sqrt{3}$ and $\omega^4 = 7-4\sqrt{3}$. Substituting for $\omega(Q)$ in (4) yields the image point of Q in R^3 with the coordinates

$$x(Q) = 0,\ y(Q) = -aK'/2\sqrt{2},\ z(Q) = 0. \tag{5}$$

The normalization constant is therefore

$$\kappa = 2a/K'. \tag{6}$$

It is strictly positive and its value is directly proportional to the edge length of the bounding cell. Substitution of (6) into (4) gives the full parametric equations for the P patch in R^3.

4. Properties of the P surface

Eqs. (4a), (4b), (4c) and (6) can be used to evaluate a number of geometric properties of the P surface. The singular points of the Weierstrass function (2), O and P are mapped into the points $O'(0,0,0)$ and $P'(0,-a/\sqrt{2},0)$ on the surface. Geometry dictates that the point P' divides the body diagonal of the bounding cell in the 1:1 ratio (Fig. 1b), while the point O' divides the cube edge, a, in the same ratio. The length $O'P'$ is an invariant of the surface with value $a/\sqrt{2}$. There is, however, no simple algebraic expression for the coordinates of the singular point Q.

By setting $\theta = 0$ in (1) we obtain the patch of the D surface, conjugate to the P patch. The corresponding image points O'' and P'' have the coordinates $O''(0,0,0)$, $P''(aK/\sqrt{2}K',0,aK/\sqrt{2}K')$. The length $O''P''$ bisects the body diagonal of the cube of side a_D in one-half (see Fig. 2). We therefore deduce that

$$a_D = aK/K'. \tag{7}$$

This relationship enables us to derive exact analytical formulae for the perimeter $\mathscr{P}$, the surface area $\mathscr{A}$ and the normalized surface-to-volume ratio $\mathscr{A}/\mathscr{V}^{2/3}$ (since the ratio must be dimensionless we take $\mathscr{V}^{2/3}$ instead of $\mathscr{V}$) of the P patch.

The Bonnet transformation preserves the metric, the area and perimeter of all associate patches. The patch perimeter $\mathscr{P}$ can therefore be simply evaluated from the associate D surface, since this patch is bounded by straight lines which the surface embeds. From Fig. 2 and using (7) we find that

$$\mathscr{P} = a_D(\sqrt{2}+1) = aK(\sqrt{2}+1)/K'. \tag{8}$$

If the area of the minimal surface bounded by a tetrahedron is $\mathscr{A}$, r is the inradius of a sphere which touches each face of that tetrahedron at one point (the inradius of the tetrahedron) and the length of the perimeter is $\mathscr{P}$, then [33]

$$\mathscr{A} = \mathscr{P}r/2. \tag{9}$$

The Coxeter cell of the P patch is the tetragonal disphenoid with inradius $r = a_P(\sqrt{2}-1)/2$. Thus, by substituting for τ and $\mathscr{P}$ in (9) and using (7), we

find $\mathscr{A} = a^2K/4K'$. The volume of the quadrirectangular tetrahedron enclosing the P patch is $a^3/3$, so

$$\mathscr{A}/\mathscr{V}^{2/3} = (3/4)^{2/3}K/K' = 0.6452799262\ldots$$

(for the fundamental patch)

$$\mathscr{A}/\mathscr{V}^{2/3} = 3K/K' = 2.345102884\ldots$$

(for the bcc unit cell).

5. Computation of the P surface

An exact computation of the P surface proceeds as follows. The evaluation of the elliptic functions given above is fast and straightforward. The Mathematica program (Wolfram Research) has elliptic functions built in as user-callable subroutines.

The Cartesian coordinates of the points of the P patch were computed using Eqs. (5) and (7) from a 10×10 mesh (Fig. 3b). The coordinates of the full P patch were obtained by reflection of the image points of the integration domain (Fig. 3) in the zx plane, a mirror plane of symmetry of the P patch. This avoids computational difficulties in the calculation of the surface coordinate corresponding to the complex plane point $\omega = (1 - 1/\sqrt{2})(1 + i)$. Larger surface pieces are conveniently calculated by transforming the coordinate system to that of Fig. 1a by a rotation of $-\pi/4$ about the z axis, reflecting in the yz plane and translating the origin along the vector $(0,1/2,1)$. The effect is the creation of a new coordinate frame with origin at M_1 whose edges M_1M_2, M_1M_4 and M_1M_5 determine the x', y' and z' axes respectively (see Fig. 4a). Hence the entire bounding cell is in the first octant and three of its faces are coordinate planes. The new coordinates of the P patch are those of P_1 (see Table 1). By reflecting a piece of the P surface obtained in this way (Fig. 4a) through the coordinate planes (a simple change of the sign of the coordinates) we arrive at the complete P unit cell (Fig. 4b).

6. Conclusions

Integration of the Enneper–Weierstrass representation of the P minimal surface with the Weierstrass function of the form $R(\tau) = \frac{1}{\sqrt{\tau^8 - 14\tau^4 + 1}}$ and the Bonnet angle of $\theta = 90°$ (with respect to the D surface) enabled us to obtain analytical expressions for the Cartesian coordinates of the fundamental patch of the surface. The surface-to-volume ratio of the fundamental patch is $0.6452799262\ldots$. Symmetry considerations allowed us to construct a piece of the surface composed of six fundamental patches, and finally the cubic unit cell of the surface composed of 48 fundamental patches.

References

[1] M.P. do Carmo, Differential Geometry of Curves and Surfaces, Prentice-Hall, Engelwood Cliffs, NJ, 1976.
[2] S. Hyde, S. Andersson, K. Larsson, Z. Blum, T. Landh, S. Lidin, B.W. Ninham, The Language of Shape. The Role of Curvature in Condensed Matter: Physics, Chemistry and Biology, Elsevier, Amsterdam, 1997.
[3] H.U. Nissen, Science 166 (1969) 1150.
[4] F.J. Almgren, Math. Intelligencer 4 (1982) 164.
[5] M. Kemp, Nature 389 (1997) 919.
[6] C.T. Kresge, M.E. Leonowicz, W.J. Roth, J.C. Vartuli, J.S. Beck, Nature 359 (1992) 710.
[7] M.E. Davis, Nature 364 (1993) 391.
[8] D.M. Anderson, P. Ström, Physica A 176 (1991) 151.
[9] P. Barois, D. Eidam, S.T. Hyde, in: E. Dubois-Violette, B. Pansu (Eds.), International Workshop on Geometry and Interfaces, Colloque de Physique No. 7, J. Phys. (Paris), vol. 51, (supplement to No. 23), Les Éditions de Physique, Les Ulis, France, 1990, p. 25.
[10] H.G. von Schnering, R. Nesper, Angew. Chem. Intern. Ed. Engl. 26 (1987) 1059.
[11] H.G. von Schnering, R. Nesper, Z. Phys. B 83 (1991) 407.
[12] H. Terrones, A.L. Mackay, Chem. Phys. Lett. 207 (1993) 45.
[13] A.L. Mackay, H. Terrones, Nature 352 (1991) 762.
[14] B. de Kruijff, Nature 386 (1997) 129.
[15] Y. Bouligand, in: E. Dubois-Violette, B. Pansu (Eds.), International Workshop on Geometry and Interfaces, Colloque de Physique No. 7, J. Phys. (Paris), vol. 51, (supplement to No. 23), Les Éditions de Physique, Les Ulis, France, 1990, p. 35.
[16] T. Landh, Fed. Eur. Biochem. Soc. (FEBS) Lett. 369 (1995) 13.
[17] V. Luzzati, P.A. Spegt, Nature 215 (1967) 701.
[18] P.J.F. Gandy, D. Cvijovic', A.L. Mackay, J. Klinowski, Chem. Phys. Lett. 314 (1999) 543.
[19] P.J.F. Gandy, J. Klinowski, Chem. Phys. Lett. (2000), in press.
[20] D. Cvijovic', J. Klinowski, J. Phys. (Paris) I 2 (1992) 137.
[21] J.C.C. Nitsche, Lectures on Minimal Surfaces, vol. 1, Cambridge University Press, Cambridge, 1989.

[22] D. Cvijovic', J. Klinowski, J. Phys. (Paris) I 2 (1992) 2207.
[23] D. Cvijovic', J. Klinowski, J. Phys. (Paris) I 2 (1992) 2191.
[24] D. Cvijovic', J. Klinowski, J. Phys. (Paris) I 3 (1993) 909.
[25] D. Cvijovic', J. Klinowski, Chem. Phys. Lett. 226 (1994) 93.
[26] A.H. Schoen, Infinite Periodic Minimal Surfaces Without Self-Intersections, NASA Technical Note D-5541, NASA, 1970.
[27] A. Fogden, S.T. Hyde, Acta Crystallogr. A 48 (1992) 575.
[28] H.S.M. Coxeter, Regular Polytopes, 2nd edn., Macmillan, New York, 1963.
[29] H.A. Schwarz, Gesammelte Mathematische Abhandlungen, Julius Springer, Berlin, 1890.
[30] M. Abramowitz, I.A. Stegun, Handbook of Mathematical Functions, Dover, New York, 1980.
[31] I.S. Gradshteyn, I.M. Ryzhik, Tables of Integrals, Series and Products, Academic Press, New York, 1980.
[32] J. Spanier, K.B. Oldham, An Atlas of Functions, Springer, Berlin, 1987.
[33] B. Smyth, Inventiones Math. 76 (1984) 411.